

# Three-Dimensional Simulation of the University of Hawai‘i FEL Oscillator: Superradiant Emission and Cavity Desynchronization

Amir Weinberg, Levi Fisher, and Siqi Li\*

*Department of Physics and Astronomy,*

*University of Hawai‘i at Mānoa, Honolulu, HI 96822, USA*

(Dated: October 17, 2025)

## Abstract

In this paper, we investigate superradiant emission in a free-electron laser (FEL) oscillator using a comprehensive three-dimensional time-dependent simulation tool. Using beam parameters from the University of Hawai‘i (UH) at Mānoa FEL facility, our study shows that at nominal bunch length, the FEL radiation exhibits superradiant scaling in saturation. We then explore how cavity desynchronization enhances this regime by mitigating the laser lethargy effect in oscillators and improving overlap between the electron bunch and the radiation pulse, with peak power increased by more than a factor of five. Finally, we simulate a short-bunch operational mode with bunch length comparable to the slippage length, which accelerates saturation and further amplifies the FEL power. These findings highlight that the UH Mānoa FEL oscillator has the potential to achieve superradiant emission at its nominal operating mode, and that short-bunch operation offers further enhancement while requiring additional optimization.

## I. INTRODUCTION

Free-electron lasers (FELs) are powerful light sources capable of generating high-power, tunable radiation spanning wavelengths from the infrared (IR) to the x-ray regime. Among different types of FEL configurations, oscillator-based systems offer unique advantages, including phase-stable pulse trains and narrow spectral bandwidth, where the radiation pulse interacts with a fresh electron bunch after each roundtrip in the oscillator cavity. These features make FEL oscillators attractive for applications such as precision spectroscopy and coherent spectroscopy [1–5].

The dynamics of FEL oscillators differ significantly from those of single-pass amplifiers due to the cavity feedback mechanism and the multi-pass evolution of the optical pulse. Understanding phenomena such as superradiant emission, cavity desynchronization, saturation dynamics in oscillators requires detailed, time-dependent modeling. Recent advances in generating extremely short, high-power x-ray FEL pulses [6] have motivated theoretical development and three-dimensional (3D) simulation efforts to investigate soliton-like superradiant behavior in amplifier FELs in saturation [7]. In FEL oscillators, a similar spiking behavior was observed in early experiments operating in the low-gain, highly sat-

---

\* [siqili@hawaii.edu](mailto:siqili@hawaii.edu)

urated regime [8, 9]. Recent interest in short-bunch superradiance for IR FEL oscillators also highlights the need for high-fidelity 3D simulation tools that can accurately model the interactions between the radiation and the electron bunch over many cavity round-trips [10].

While simulation codes such as **GENESIS** [11], **GINGER** [12], and **PUFFIN** [13] have been widely used for FEL modeling, they each present limitations for oscillator studies. **GENESIS** and **PUFFIN** employ fully 3D field solvers, whereas the original **GINGER** assumed axisymmetric fields. **PUFFIN** can model strong gain and harmonic emission from first principles, but is computationally intensive and has not been widely applied to oscillator systems until recently [14]. In addition, the **MINERVA** code, in combination with the Optical Propagation Code (OPC) [15], has been applied to oscillator studies, providing a three-dimensional, time-dependent framework that includes optical propagation in the cavity and can treat both high-Q and low-Q regimes [16]. These developments highlight the growing ability of modern FEL simulation tools to handle oscillator physics, but also the continuing need for flexible infrastructures that can be adapted to different facilities and experimental configurations.

In this paper, we present a 3D simulation framework for FEL oscillators using a developmental version of the new **GINGER-3D** code, a major revision of the original **GINGER** code [12], including a fully Cartesian x-y Alternating-Direction-Implicit radiation field solver in the transverse plane. We have developed an external pulse propagation module in **Matlab** that couples the near-field radiation output of **GINGER-3D** and models cavity geometry and mirror optics, providing flexibility for implementing advanced features such as inserting additional optics for interferometric configurations to achieve phase coherence [17–19].

As a first demonstration, we apply this simulation framework to the FEL oscillator using baseline parameters from the University of Hawai‘i (UH) at Mānoa’s FEL facility. Originally developed by John Madey, the facility was designed with the capability of generating IR radiation via FEL interaction and x-ray radiation via inverse Compton scattering of the electron beam and the IR photons [20]. Although it has been inactive for several years, current efforts focus on re-commissioning both the accelerator and the FEL, alongside supporting simulation and design studies [21, 22].

Our simulation results using the nominal parameters of the UH FEL demonstrate superradiant emission in saturation, showing the expected superradiant scaling of radiation energy linearly proportional to the square of the number of electrons.

We also investigate the effect of cavity desynchronization. A cavity is considered perfectly

synchronized when the round-trip time of the radiation pulse matches an integer multiple of the electron bunch repetition period. However, during the FEL interaction, the radiation pulse slips ahead of the electron bunch, and the amplification process effectively slows the group velocity of the radiation pulse compared to its speed in vacuum. In the context of FEL oscillators, this is known as the laser lethargy effect [23]. By slightly shortening the cavity length, i.e. introducing desynchronization, the interaction between the radiation and the electron bunch can be sustained throughout the gain process [24]. At saturation, the group velocity of the radiation catches up as the gain slows down, suggesting that dynamic desynchronization would be ideal to optimize both gain buildup and saturated power [25]. This has previously been achieved by modulating the electron bunch repetition rate within a macropulse using fast RF phase shifters, without physically changing the cavity length [25, 26]. However, such phase shifters are not currently available at the UH Mānoa facility. Therefore, in our simulation study, we implement desynchronization by shortening the cavity length by a fixed amount. We determine the optimal desynchronization by identifying the case that maximizes either peak power or pulse energy.

Our simulation results show that at the desynchronization value corresponding to the optimal peak power, the radiation power is enhanced by a factor of five compared to the perfectly synchronized case. Shortening of the cavity length pushes the radiation pulse towards the head of the electron bunch, allowing the electron phase space to develop the soliton-like superradiant characteristic of saturated FELs: electrons undergo synchrotron oscillations within the ponderomotive bucket, such that the head of the bunch transfers energy to the radiation pulse while the tail gains energy from it. This results in a reduced pulse duration and the formation of trailing secondary peaks, a well-known spiking behavior observed in highly saturated FEL oscillators [8, 9] as well as the recent demonstration of terawatt-scale attosecond x-ray FEL pulses [6, 27].

It is important to note that in the nominal operating condition, the bunch length is 2 ps, roughly four times the radiation slippage length, corresponding to the particular situation of superradiant emission described in [28] as “periodic spiking behavior”, where the electron bunch can be conceptually divided into consecutive regions each of a slippage length. A similar behavior has been studied theoretically and numerically in [29, 30].

To illustrate superradiant emission in the short bunch regime, we simulate a case where the bunch length is roughly equal to and slightly smaller than the slippage length of the UH

FEL oscillator, a condition similar to [10, 31]. The short bunch simulation is also motivated by future upgrade plans for the UH Mānoa linac, which aim to incorporate beam manipulation and shaping techniques [32] to achieve IR absorption and vibrational spectroscopy with sub-picosecond resolution [33]. Before an explicit bunch compression mechanism is developed at the UH Mānoa linac, we only change the bunch length and keep the other machine and beam parameters the same as the nominal case in our simulation to isolate the effect of bunch length shortening. Realistically, strong bunch compression likely increases the slice energy spread, and incorporating such effects will be the subject of future work in coordination with linac upgrade design studies.

In the short bunch case, the leading portion of the bunch produces a strong spike that dominates the radiation profile. However, because the bunch length is only comparable to, rather than much shorter than, the slippage length, residual overlap between the radiation and the bunch tail, enhanced by cavity desynchronization, allows a smaller secondary peak to develop. This differs from the long-pulse “periodic spiking” behavior in that only one dominant spike is sustained, while secondary structures remain weak. Our simulation results show that with the short electron bunches, the FEL reaches saturation significantly faster, and the output power is enhanced compared to nominal bunch length. Furthermore, the effect of desynchronization is also stronger. The peak power improves by a factor of 17 when optimally desynchronized compared to perfect synchronization.

The paper is organized as follows. Section II describes the simulation tool and the beam and cavity parameters at the UH Mānoa FEL facility and demonstrates the simulation results of the nominal bunch operation. Section III presents the simulation results with nominal bunch length while implementing cavity desynchronization. Section IV presents the simulation results of the short-bunch operation along with the effects of cavity desynchronization. Section V offers concluding remarks and future research directions.

## II. THE UH FEL OSCILLATOR SIMULATION

For the FEL interaction, we use the newly developed **GINGER-3D**, which offers radiation propagation capabilities similar to those of **GENESIS**, but is expected to be faster due to its Fortran 2003/2008 code base, in contrast to the C++ implementation of **GENESIS**. **GINGER-3D** also outputs data in HDF5 format, enabling seamless post-processing with stan-

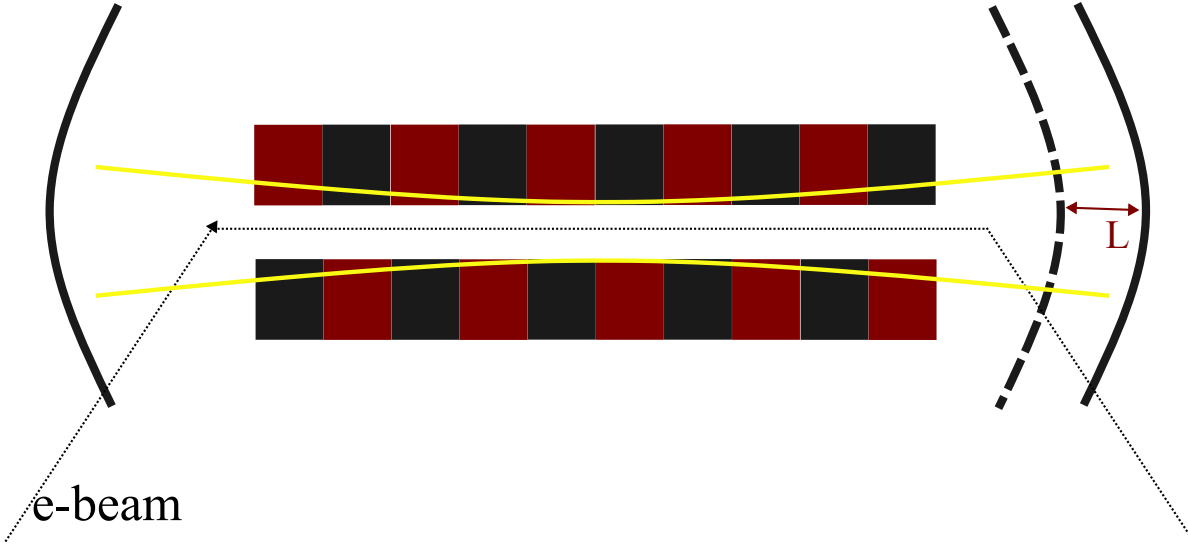


FIG. 1: Schematic of the FEL cavity.

dard tools such as **Python** and **MATLAB**.

To model radiation propagation outside the undulator, we have implemented a separate propagation module employing Fourier-optics-based free-space diffraction and mirror boundary conditions. After each undulator pass, the output field from **GINGER-3D** is passed to this code, which simulates free-space propagation and reflection from the cavity mirrors. In the Fourier optics model, each mirror is approximated as a focusing lens with a focal length equal to half of its radius of curvature. The pulse propagation code is modular and allows convenient modification of cavity configurations, including asymmetric mirror reflectivity and the insertion of Michelson resonator and Fox-Smith resonator, to explore potential 3D effects in FEL oscillators. The propagated field is then re-injected into **GINGER-3D** for the next round-trip simulation. The **Matlab** code package for pulse propagation can be found on [34].

The FEL system at UH Mānoa consists of a thermionic microwave gun that produces electrons with macropulses of  $4\text{-}5\ \mu\text{s}$  duration at a 4 Hz repetition rate. Each macropulse contains micropulses at 2.856 GHz, set by the RF system. The linear accelerator (linac) accelerates the beam up to 45 MeV. At the FEL cavity entrance, the electron bunch can reach a full-width at half-maximum (FWHM) duration around 2 ps [20]. The FEL uses a Mark V planar undulator and an optical cavity tuned to operate near  $3\ \mu\text{m}$  [35].

Table I summarizes the machine settings and beam parameters. Because the machine is

TABLE I: Parameters of the UH Mānoa FEL.  $\Delta L$  indicates the shortening of the cavity length to implement cavity desynchronization.

Parameter	Value	Units
<b>e-beam</b>		
Beam energy	40	MeV
Energy spread	0.5	%
Normalized emittance $\epsilon_{n,x}$ , $\epsilon_{n,y}$	8	$\pi\text{-mm-mrad}$
Bunch duration FWHM	2 (nominal), 0.5 (short bunch)	ps
Current Peak	30 (nominal), 120 (short bunch)	A
Twiss parameter $\beta_x$	1.4	m
Twiss parameter $\beta_y$	0.24	m
Twiss parameter $\alpha_x$	0.47	rad
Twiss parameter $\alpha_y$	0	rad
<b>Undulator</b>		
Period $\lambda_u$	2.3	cm
Number of periods $N_u$	47	
Undulator parameter $K$	1.2	
Radiation wavelength $\lambda_r$	3.2	$\mu\text{m}$
<b>Cavity</b>		
Length	2.0	m
Mirrors radius of curvature	1.3	m
Cavity loss	7	%

not operating at the time of writing, the machine settings and nominal beam parameters are taken from past measurements [20, 35]. The Twiss parameters are estimated based on the matching requirement. In the vertical plane, the beam is assumed to be at its waist and remain collimated throughout the undulator, so we require  $\alpha_y = 0$  and  $\beta_y = \frac{\gamma\lambda_u}{2\pi K}$  [36], where  $\gamma$  is the relativistic Lorentz factor. In the horizontal plane, the waist is assumed to occur at the center of the undulator, with the horizontal beam size matched to the radiation beam size. The Rayleigh range  $Z_R$  of the radiation is approximately half of the undulator length,

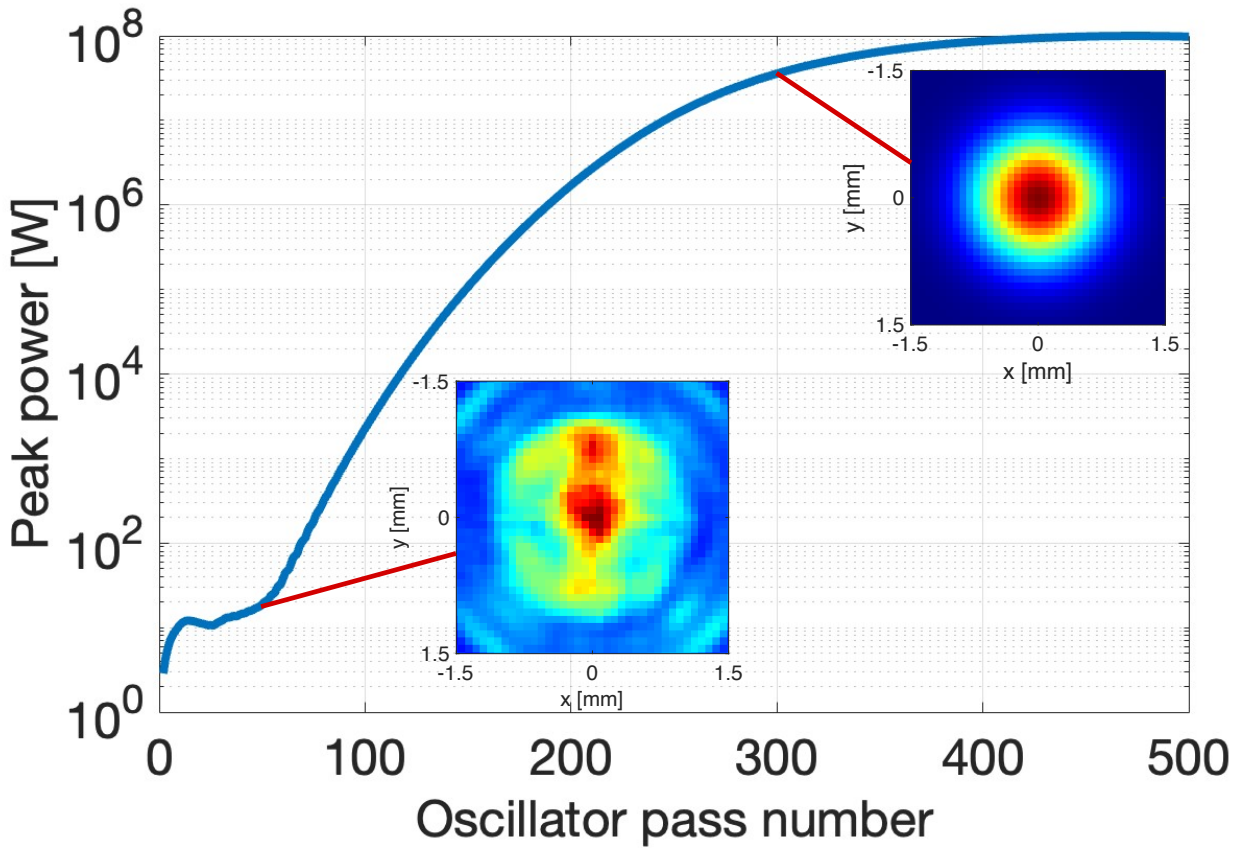


FIG. 2: Peak radiation power as a function of oscillator passes, using the nominal beam and machine parameters. We show the integrated transverse profile of the radiation at pass 50 and pass 300. Note that the colorbars are normalized to have a maximum of 1 for both profiles.

ensuring strong overlap with the electron beam. Therefore, using  $\sigma_x \sim \sigma_r = \sqrt{\frac{\lambda_r}{4\pi} Z_R}$ , we set  $\beta_x$  by  $\beta_x = \sigma_x^2/\epsilon_x$ , where  $\epsilon_x$  is the geometric emittance.

Figure 2 shows the radiation power as a function of the number of round-trips through the cavity using the nominal beam and machine parameters. The radiation peak power reaches several megawatts over approximately 200 passes and reaches saturation around 400 - 500 passes. We limit the maximum pass number to 400 in the numerical simulations because it corresponds to about 5  $\mu$ s of macropulse, longest macropulse duration delivered at the UH Mānoa linac, limited by the pulse forming network and back-bombardment effect on the cathode [37]. Inset plots show the integrated transverse profile of the radiation

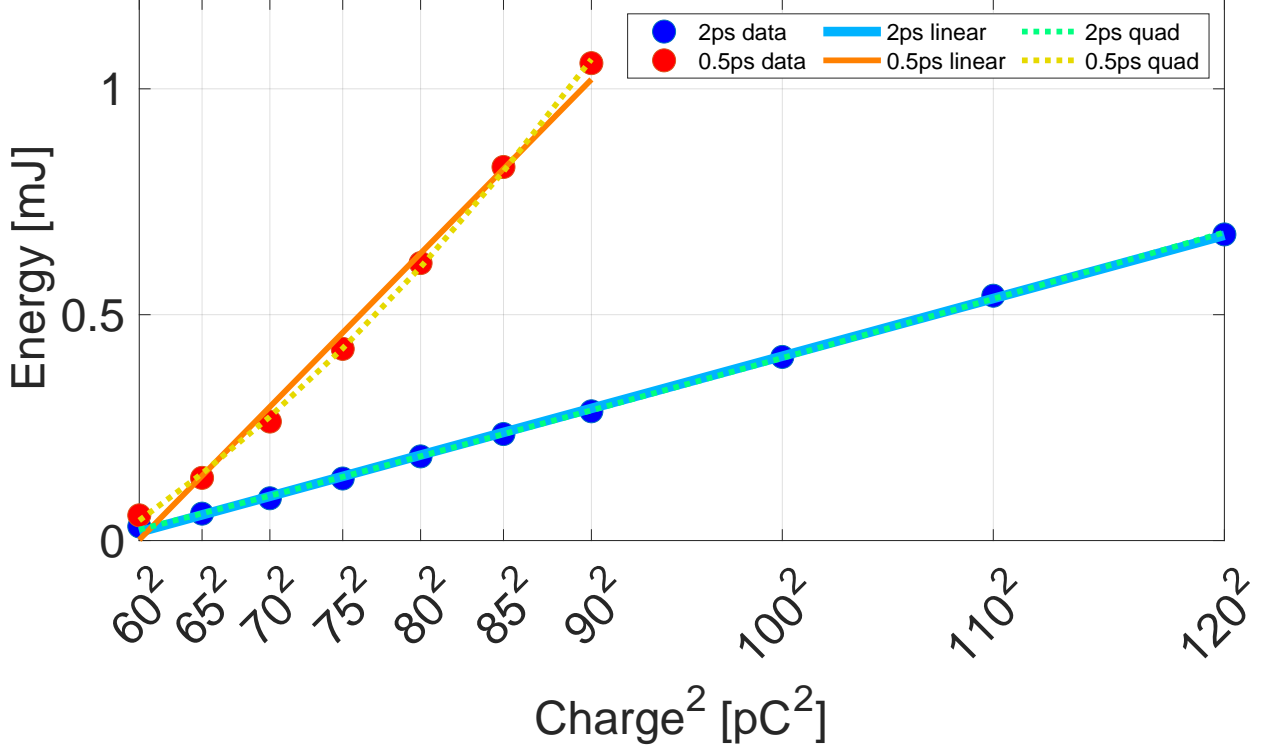


FIG. 3: Radiation energy vs. charge squared for the 2 ps bunch length case and the 0.5 ps bunch length case, both for 400 oscillator passes and at perfect synchronization. Simulation data are presented with solid dots, and polynomial fittings using charge squared are presented with solid and dashed lines for linear and quadratic fittings respectively.

pulse at pass 50 and pass 300 respectively, highlighting the spatial structure captured by our 3D simulation framework. Note that earlier publication reported design peak power of 2.6 MW [20], while our nominal case gives  $\sim$ 80 MW of simulated peak power. The difference reflects uncertainties in archived machine parameters and knowledge gap given the history of the lab. In this paper, we focus on potential performance under idealized conditions.

To demonstrate the superradiant scaling of radiation energy  $\propto N_e^2$ , where  $N_e$  is the number of electrons, we increase the electron charge in the simulation and observe a linear dependence of the radiation pulse energy on charge squared in Fig. 3, consistent with the expected superradiant scaling [38]. Fitting with both linear and quadratic polynomials shows that the 2 ps case follows primarily linear scaling with charge squared.

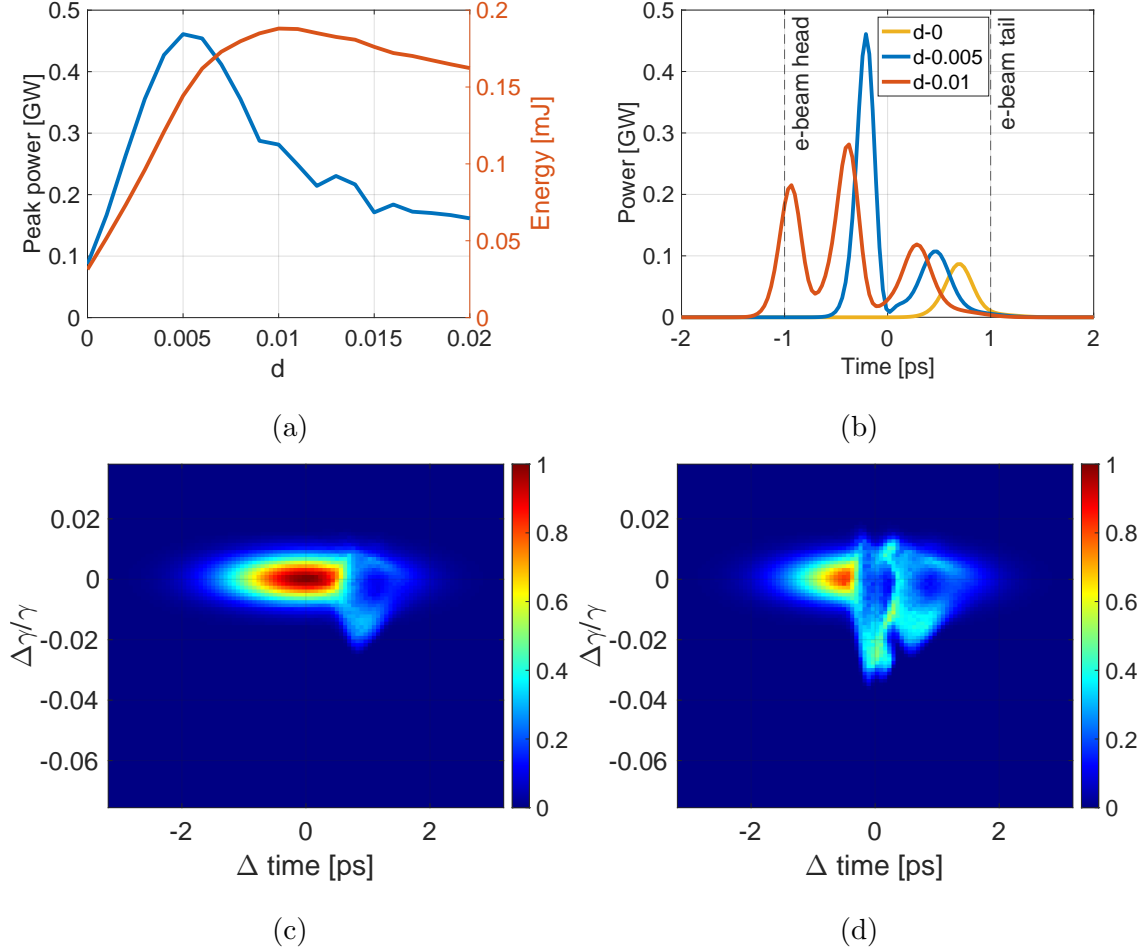


FIG. 4: (a) Peak power (blue) and pulse energy (red) at oscillator pass 400 as a function of varying desynchronization values  $d$ . (b) Pulse profiles for perfect synchronization  $d = 0$  (yellow), optimal  $d = 0.005$  based on peak power (blue), and optimal  $d = 0.01$  based on pulse energy (red). The FWHM of the electron bunch length is indicated by the dashed vertical lines. (c) Electron phase space after pass 400 for perfect synchronization ( $d = 0$ ). (d) Electron phase space after pass 400 for the optimal desynchronization based on peak power ( $d = 0.005$ ). Phase space images are normalized by their total sums. Time axes in (c) and (d) have been offset to position the electron beam at the center.

### III. DESYNCHRONIZATION SIMULATION

As discussed in Sec. I, cavity desynchronization is introduced to mitigate the laser lethargy effect in FEL oscillators. We define the desynchronization value,  $d = 2\Delta L/S$ , where  $S = N_u\lambda_r$  is the slippage length, and  $\Delta L$  is illustrated in Fig. 1. In our simula-

tion, we implement this by shifting the radiation filed in GINGER-3D by  $2\Delta L$  during the free-space propagation before re-injection into the undulator. We scan a range of desynchronization values and identify the optimal configurations based on peak power and pulse energy (see Fig. 4(a)). Figure 4(b) shows the radiation pulse profiles after 400 passes for several desynchronization values. The overall effect of desynchronization, or cavity shortening, is clearly illustrated by the radiation pulse slipping more and more towards the head of the electron bunch as seen in Figure 4(b). At the optimal desynchronization based on peak power,  $d = 0.005$ , the peak power is enhanced by more than a factor of five compared to the perfectly synchronized case ( $d = 0$ ). This optimal value, corresponding to about  $0.1\lambda_r$  is consistent with theoretical predictions [39] and experimental results [25]. This enhancement results from improved temporal overlap between the radiation pulse and electron bunch throughout the amplification process. These optimal desynchronization values of  $d = 0.005$  based on peak power and  $d = 0.01$  based on pulse energy correspond to a movement of the downstream cavity mirror on the order of 0.4-0.8  $\mu\text{m}$ , which is achievable in experiments using piezo-driven translation stages.

As shown in Fig. 4(b), while the pulse profile in the perfectly synchronized case resembles a smooth Gaussian, the optimal desynchronization leads to the formation of a sharp leading peak followed by a trailing peak. Multiple peaks are generated because the leading radiation peak slips ahead of the electron bunch while the interaction of the remaining electrons with the radiation field evolves into a trailing peak, consistent with the soliton-like superradiance [6] or spiking behavior [8, 9] previously reported in highly saturated FELs. This behavior is the most prominent for larger desynchronization as seen in the  $d = 0.01$  curve in Fig. 4(b) where three peaks are formed.

We observe pulse shortening of the leading spike with desynchronization: the FWHM decreases from 0.31 ps ( $d = 0$ ) to 0.29 ps ( $d = 0.01$ ) and 0.20 ps ( $d = 0.005$ ) in Fig. 4(b). Furthermore, all measured widths are below the slippage length ( $S = N_u\lambda_r = 0.51$  ps), consistent with the periodic spiking superradiant dynamics. The separation between the individual spikes for higher desynchronization,  $d = 0.01$  is 0.59 ps, and that for the lower and optimal desynchronization,  $d = 0.005$ , is 0.69 ps. Although spikes in periodic spiking are often separated by the slippage length [28, 29], in an oscillator with non-zero desynchronization the spike-to-spike separation reflects where the optical pulse enters the bunch each pass and where secondary spikes form. For larger desynchronization, the pulse interacts

with the bunch head and consecutive spikes form on fresh electrons, giving separations close to the slippage length. For smaller desynchronization, the pulse begins nearer the bunch center, so the region just behind the leading spike has already lost energy, reducing local gain. The next spike therefore forms later, yielding a larger spike-to-spike separation, as indicated in the  $d = 0.005$  case.

We examine the electron phase space evolution after the final pass for perfect synchronization (Fig. 4(c)) and that for the optimal desynchronization (Fig. 4(d)) based on peak power. For perfect synchronization, it is clear that the radiation only builds up towards the tail of the electron bunch, a demonstration of the laser lethargy effect. In the optimal desynchronization where multiple peaks have developed in saturation, the electron bunch undergoes synchrotron oscillations within the ponderomotive bucket. This manifests as energy exchange across the bunch: the head loses energy to the radiation pulse, while the tail absorbs energy from it.

Although peak power and pulse energy peak at different  $d$  (Fig. 4(a)), both increase rapidly from zero desynchronization. Peak power falls more sharply after optimum, while pulse energy remains elevated due to the contribution of trailing spikes (see Supplemental Material [URL will be inserted by publisher] SM2psd0p01.mp4).

#### IV. SHORT-BUNCH OPERATION WITH DESYNCHRONIZATION

To further investigate superradiant emission in the short bunch regime, we simulate FEL oscillator operation using a shorter electron bunch with a FWHM duration of 0.5 ps, which is slightly smaller than the slippage length 0.51 ps. Achieving this shorter bunch length experimentally is a key goal of the planned upgrade to the UH Mānoa FEL facility. It may be realized through a combination of thermally-assisted photoemission for enhanced cathode performance [40], bunch compression via existing magnetic chicanes, laser-based beam shaping using a synchronized optical laser with a spare undulator available in the lab [41], and accelerator-based machine learning algorithms for beam optimization [42].

Note that we set the simulation time slice to be about three times the resonant radiation period. This choice is consistent with the slowly-varying envelope approximation employed by **GINGER-3D**, in which the field envelope varies on timescales longer than the radiation period. In the short bunch case, the FEL reaches saturation significantly faster than in the

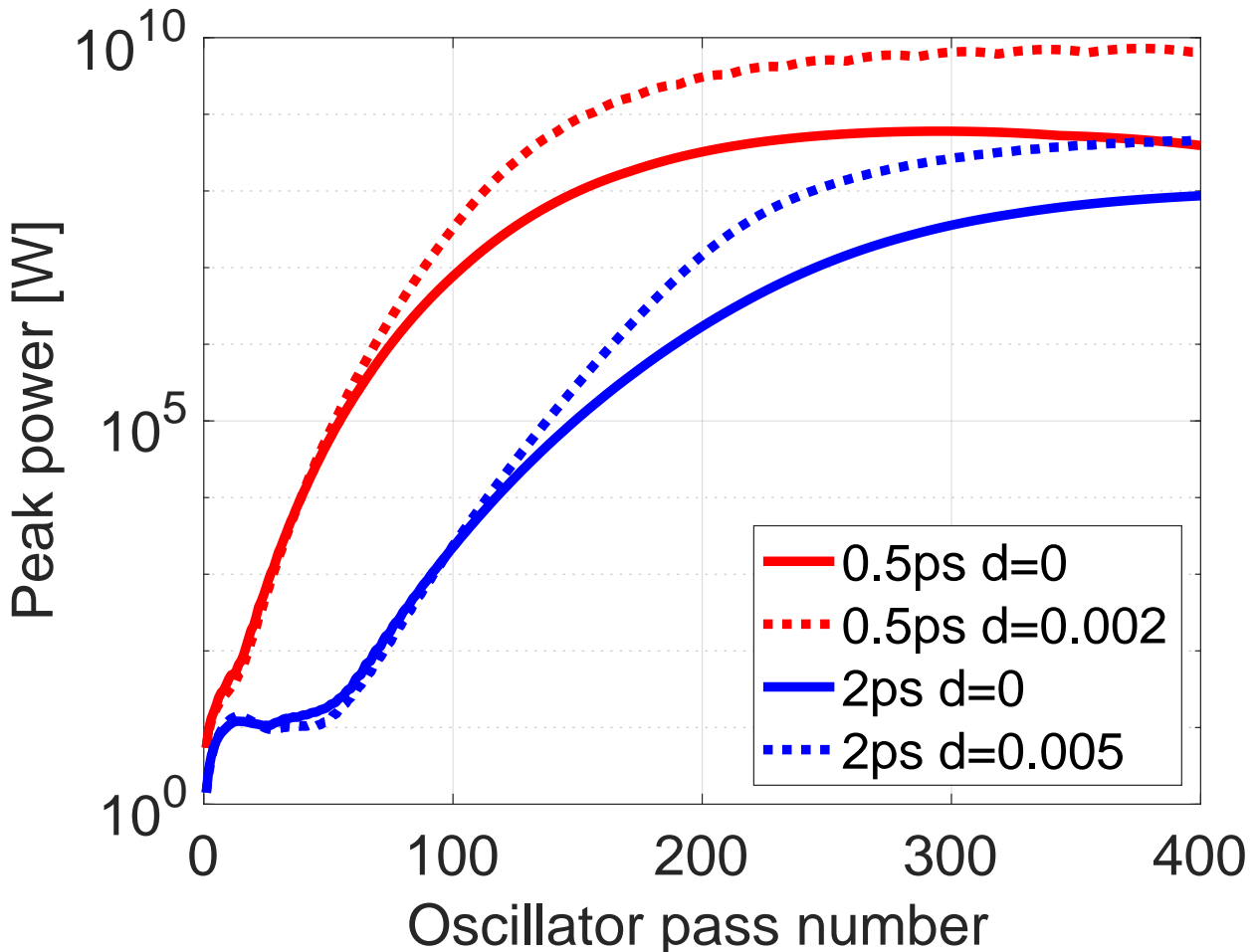


FIG. 5: Peak radiation power as a function of oscillator passes, for 2 ps bunch length at zero (dashed) and optimal (solid) desynchronization  $d = 0.005$  (blue) and 0.5 ps bunch length at zero (dashed) and optimal (solid) desynchronization  $d = 0.002$  (red).

nominal 2 ps case, as shown in Fig. 5. Even in perfect synchronization, the peak power increases from 86 MW in the 2 ps case to 392 MW in the 0.5 ps case.

We repeat the desynchronization scan described in Sec. III to determine the optimal cavity length shortening for the short-bunch configuration. The optimal desynchronization is found to be  $d = 0.002$  both based on peak power and pulse energy (see Fig. 6(a)), more than a factor of two smaller than that for the 2 ps case under the same machine and beam conditions. Because the short bunch saturates more quickly, the simulation after 400 passes represents a regime where gain is slowed and the lethargy effect has already relaxed. This result underscores the importance of dynamic desynchronization for short-bunch operation, which we will explore in future work.

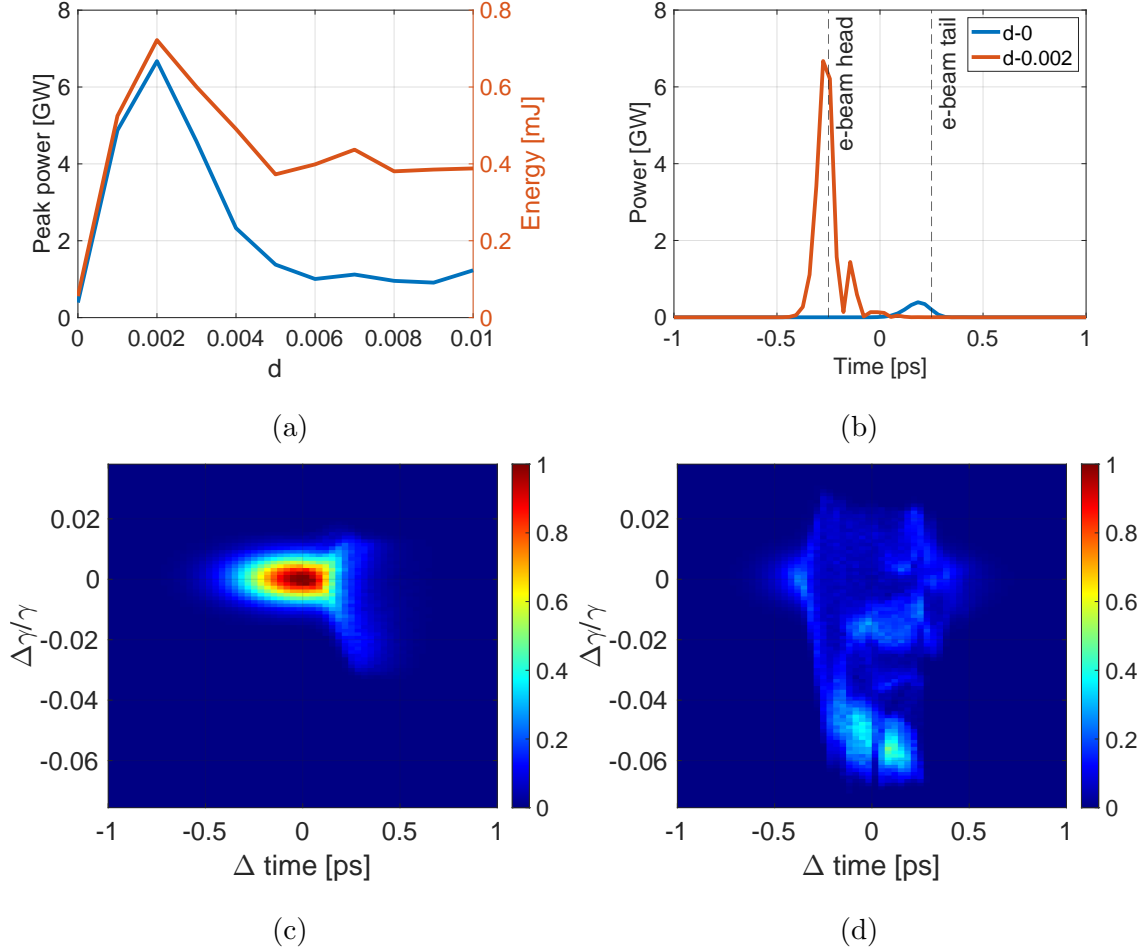


FIG. 6: (a) Peak power (blue) and pulse energy (red) at pass 400 as a function of varying desynchronization values  $d$ . (b) Pulse profiles for perfect synchronization  $d = 0$  and optimal desynchronization  $d = 0.002$  based on both the peak power and pulse energy. The FWHM of the electron bunch length is indicated by the dashed vertical lines. (c) Electron phase space after pass 400 for perfect synchronization ( $d = 0$ ). (d) Electron phase space after pass 400 for the optimal desynchronization ( $d = 0.002$ ). Phase space images are normalized by their total sums. Time axes in (c) and (d) have been offset to position the electron beam at the center.

Figure 6(b) shows the radiation pulse profile at saturation corresponding to two different desynchronization values. For optimal desynchronization, the pulse profile exhibits a leading peak and a weak trailing peak, similar to the pulse profile in the 2 ps case at optimal desynchronization (Fig. 4(b)). The FWHM of the leading peak is 0.09 ps for  $d = 0.002$ , and

that of the perfect synchronization case is 0.13 ps. The optimal peak power is enhanced by more than an order of magnitude compared to the 2 ps bunch length case at the optimal desynchronization. We see that in Fig. 6(d) the maximum energy loss of the electrons is above 6% for the 0.5 ps case, whereas for the 2 ps case the maximum energy loss is about 3% (Fig. 2(d)). The evolution of the radiation pulse profile and the electron phase space (SM0p5psd00002.mp4) is illustrated in the Supplemental Material at [URL will be inserted by publisher].

Unlike the 2 ps bunch length desynchronization scan, as shown in Fig. 6(a), we see the dependence of the peak power and the pulse energy on the desynchronization value is similar. This is because in the short bunch scenario, the bunch length only allows for one dominant spike followed by a weak trailing spike to develop instead of the multiple spikes as shown in Fig. 4(b), making both the peak power and pulse energy similarly sensitive to the desynchronization values.

We also plot the pulse energy dependence on charge squared for the short bunch case in Fig. 3. It is important to note that in this figure, we use perfect synchronization for all cases. As the charge increases, the FEL gain changes, which in turn shifts the optimal desynchronization value, indicating that for each different charge, there will be a different optimal desynchronization. Nonetheless, we observe that without tuning  $d$ , the 2 ps case already exhibits the expected superradiant scaling, confirming that nominal operation is superradiant. For the 0.5 ps short-bunch case, we fixed  $d = 0$  for consistency and limited the scan to 90 pC, as higher charge at this short bunch duration would introduce additional effects, such as increased energy spread, beyond the scope of the present comparison. Within this range, the short bunch shows a convex quadratic dependence on charge squared, reflecting its greater sensitivity to cavity timing and radiation build-up. In addition, the short bunch extracts energy more efficiently, as seen in the steeper slope compared to the 2 ps case. These results motivate the integration of machine-learning-based optimization into the simulation framework to dynamically identify the optimal desynchronization along with multiple other machine parameters, such as bunch charge, bunch length, and compression settings. Future work will also include convergence testing (e.g., increasing time resolution at high charges) to rule out numerical artifacts, as well as exploring dynamic desynchronization within a macropulse.

## V. CONCLUSIONS

In conclusion, we have developed and demonstrated a comprehensive simulation framework for modeling the FEL oscillator at the University of Hawai‘i at Mānoa. Our results indicate that this facility is capable of producing superradiant emission given by the nominal beam and machine parameters. Furthermore, by implementing cavity desynchronization and future upgrade to short bunch operation, we can significantly enhance the peak power of the FEL. This finding opens up new possibilities for high-peak-power and ultrafast pulse generation at UH Mānoa. The simulation tool has also proven to be flexible and adaptable to a variety of beam parameters, making it a valuable platform for design and optimization efforts. Ongoing simulation work includes benchmarking the results with other FEL codes such as PUFFIN and MINERVA in combination with our pulse propagation code package. Looking forward, current efforts on reviving the facility will make it possible to experimentally verify the results of our simulations and demonstrate superradiance operation. Furthermore, this simulation framework enables detailed studies of advanced optical configurations, such as interferometric setups for imposing phase coherence on the output pulses, as well as systematic investigations into cavity length tuning for maximizing FEL output power, extraction efficiency, and bunch length optimization to support future beamline upgrades.

## ACKNOWLEDGMENTS

The authors acknowledge William Fawley for helpful discussions. Work on the GINGER-3D code is supported by the U.S. Department of Energy under Contract 218 No. DE-AC02-76SF00515 to SLAC and in part by Sincrotrone Trieste. This work is supported by the U.S. Department of Energy, Office of Science, Office of Basic Energy Sciences and Office of Accelerator Research & Development and Production, under Contract No. DE-SC0025583.

---

[1] G. Ramian, The new ucsb free-electron lasers, *Nuclear Instruments and Methods in Physics Research Section A: Accelerators, Spectrometers, Detectors and Associated Equipment* **318**, 225 (1992).

[2] D. Oepts, A. Van der Meer, and P. Van Amersfoort, The free-electron-laser user facility felix, *Infrared physics & technology* **36**, 297 (1995).

[3] S. Winnerl, D. Stehr, O. Drachenko, H. Schneider, M. Helm, W. Seidel, P. Michel, S. Schneider, J. Seidel, S. Grafstrom, *et al.*, Felbe free-electron laser: Status and application for time resolved spectroscopy experiments, in *2006 Joint 31st International Conference on Infrared Millimeter Waves and 14th International Conference on Terahertz Electronics* (IEEE, 2006) pp. 159–159.

[4] W. Schöllkopf, S. Gewinner, W. Erlebach, G. Heyne, H. Junkes, A. Liedke, G. Meijer, V. Platschkowski, G. v. Helden, H. Bluem, *et al.*, The ir and thz free-electron laser at the fritz-haber-institut, in *35th International Free Electron Laser Conference* (2013) pp. 657–660.

[5] H. Zen, S. Suphakul, T. Kii, K. Masuda, and H. Ohgaki, Present status and perspectives of long wavelength free electron lasers at kyoto university, *Physics Procedia* **84**, 47 (2016).

[6] P. Franz, S. Li, T. Driver, R. R. Robles, D. Cesar, E. Isele, Z. Guo, J. Wang, J. P. Duris, K. Larsen, *et al.*, Terawatt-scale attosecond x-ray pulses from a cascaded superradiant free-electron laser, *Nature Photonics* **18**, 698 (2024).

[7] R. R. Robles, L. Giannessi, and A. Marinelli, Three-dimensional theory of superradiant free-electron lasers, *Physical Review Research* **6**, 033158 (2024).

[8] R. Warren, J. Goldstein, and B. Newnam, Spiking mode operation for a uniform-period wiggle, *Nuclear Instruments and Methods in Physics Research Section A: Accelerators, Spectrometers, Detectors and Associated Equipment* **250**, 19 (1986).

[9] B. A. Richman, J. Madey, and E. Szarmes, First observation of spiking behavior in the time domain in a free-electron laser, *Physical review letters* **63**, 1682 (1989).

[10] H. Zen, R. Hajima, and H. Ohgaki, Full characterization of superradiant pulses generated from a free-electron laser oscillator, *Scientific Reports* **13**, 6350 (2023).

[11] S. Reiche, Genesis 1.3: a fully 3d time-dependent fel simulation code, *Nuclear Instruments and Methods in Physics Research Section A: Accelerators, Spectrometers, Detectors and Associated Equipment* **429**, 243 (1999).

[12] *Proceedings of FEL* (Berlin, Germany, 2006).

[13] L. Campbell and B. McNeil, Puffin: A three dimensional, unaveraged free electron laser simulation code, *Physics of Plasmas* **19** (2012).

[14] P. Pongchalee and B. W. McNeil, Unaveraged simulations of a cavity based free electron laser, *Results in Physics* **57**, 107390 (2024).

[15] J. Karssenberg, P. J. van der Slot, I. Volokhine, J. W. Verschuur, and K.-J. Boller, Modeling paraxial wave propagation in free-electron laser oscillators, *Journal of applied physics* **100** (2006).

[16] P. J. Van Der Slot and H. P. Freund, Three-dimensional, time-dependent analysis of high-and low-q free-electron laser oscillators, *Applied Sciences* **11**, 4978 (2021).

[17] D. Oepts, R. Bakker, D. Jaroszynski, A. van der Meer, and P. van Amersfoort, Induced and spontaneous interpulse phase locking in a free-electron laser, *Physical review letters* **68**, 3543 (1992).

[18] E. B. Szarmes and J. M. Madey, The michelson resonator free-electron laser. i. passive mode structure and mode decay, *IEEE journal of quantum electronics* **29**, 452 (2002).

[19] E. B. Szarmes and J. Madey, The michelson resonator free-electron laser. ii. supermode structure and mirror detuning effects, *IEEE journal of quantum electronics* **29**, 465 (2002).

[20] P. Niknejadi, J. M. Kowalczyk, M. R. Hadmack, B. T. Jacobson, I. Howe, S. Kan, S. Smith, E. B. Szarmes, G. Varner, and J. M. Madey, Free-electron laser inverse-compton interaction x-ray source, *Physical Review Accelerators and Beams* **22**, 040704 (2019).

[21] N. Bidault, A. Weinberg, H. Purwar, and S. Li, Recommissioning of the university of hawai‘i linac and free electron laser, in *16th International Particle Accelerator Conference* (JACoW, 2025) in press.

[22] A. Weinberg, N. Bidault, and S. Li, Research plans for the university of hawai‘i accelerator and free-electron laser lab, in *16th International Particle Accelerator Conference* (JACoW, 2025) in press.

[23] W. Colson, C. Pellegrini, and A. Renieri, Free electron laser handbook, The Netherlands: North-Holland Physics (1990).

[24] W. B. Colson and A. Renieri, Pulse propagation in free electron lasers, *Le Journal de Physique Colloques* **44**, C1 (1983).

[25] R. Bakker, G. Knippels, A. van der Meer, D. Oepts, D. Jaroszynski, and P. van Amersfoort, Dynamic desynchronization of a free-electron laser resonator, *Physical Review E* **48**, R3256 (1993).

[26] H. Zen, H. Ohgaki, and R. Hajima, High-extraction-efficiency operation of a midinfrared free electron laser enabled by dynamic cavity desynchronization, *Physical Review Accelerators and Beams* **23**, 070701 (2020).

- [27] M. D. Fayer, *Ultrafast infrared and Raman spectroscopy*, Vol. 26 (CRC Press, 2001).
- [28] G. Moore and N. Piovella, Superradiant short-pulse propagation in the free-electron laser oscillator, *IEEE journal of quantum electronics* **27**, 2522 (2002).
- [29] R. Bonifacio, F. Casagrande, G. Cerchioni, L. de Salvo Souza, P. Pierini, and N. Piovella, Physics of the high-gain fel and superradiance, *La Rivista del Nuovo Cimento (1978-1999)* **13**, 1 (1990).
- [30] R. Bonifacio, N. Piovella, and B. McNeil, Superradiant evolution of radiation pulses in a free-electron laser, *Physical Review A* **44**, R3441 (1991).
- [31] A. Gover, R. Ianconescu, A. Friedman, C. Emma, N. Sudar, P. Musumeci, and C. Pellegrini, Superradiant and stimulated-superradiant emission of bunched electron beams, *Reviews of Modern Physics* **91**, 035003 (2019).
- [32] D. Cesar, A. Anakru, S. Carbajo, J. Duris, P. Franz, S. Li, N. Sudar, Z. Zhang, and A. Marinelli, Electron beam shaping via laser heater temporal shaping, *Physical Review Accelerators and Beams* **24**, 110703 (2021).
- [33] R. Kießling, S. Gewinner, A. Paarmann, W. Schöllkopf, and M. Wolf, Synchronized mid-infrared pulses at the fritz haber institute ir-fel, in *38th International Free-Electron Laser Conference (FEL2017)* (JACoW, 2018) pp. 188–191.
- [34] A. Weinberg, Oscillator add-on, [https://github.com/amirwein/oscillator\\_addon](https://github.com/amirwein/oscillator_addon) (2025).
- [35] S. V. Benson, W. S. Fann, B. A. Hooper, J. M. Madey, E. B. Szarmes, B. Richman, and L. Vintro, A review of the stanford mark iii infrared fel program, *Nuclear Instruments and Methods in Physics Research Section A: Accelerators, Spectrometers, Detectors and Associated Equipment* **296**, 110 (1990).
- [36] K.-J. Kim, Z. Huang, and R. Lindberg, *Synchrotron radiation and free-electron lasers* (Cambridge university press, 2017).
- [37] J. Kowalczyk, M. R. Hadmack, and J. M. Madey, Measurement of back-bombardment temperature rise in microwave thermionic electron guns, *Review of Scientific Instruments* **84** (2013).
- [38] R. H. Dicke, Coherence in spontaneous radiation processes, *Physical review* **93**, 99 (1954).
- [39] K.-J. Kim and M. Xie, Stability and performance of cdrl-fel, *Nuclear Instruments and Methods in Physics Research Section A: Accelerators, Spectrometers, Detectors and Associated Equipment* **304**, 146 (1991).

- [40] K. Torgasin, K. Morita, H. Zen, K. Masuda, T. Katsurayama, T. Murata, S. Suphakul, H. Yamashita, T. Nogi, T. Kii, *et al.*, Thermally assisted photoemission effect on ceb 6 and lab 6 for application as photocathodes, *Physical Review Accelerators and Beams* **20**, 073401 (2017).
- [41] S. Li, Z. Zhang, S. Alverson, D. Cesar, T. Driver, P. Franz, E. Isele, J. P. Duris, K. Larsen, M.-F. Lin, *et al.*, “beam à la carte”: Laser heater shaping for attosecond pulses in a multiplexed x-ray free-electron laser, *Applied Physics Letters* **125** (2024).
- [42] A. Edelen, N. Neveu, M. Frey, Y. Huber, C. Mayes, and A. Adelmann, Machine learning for orders of magnitude speedup in multiobjective optimization of particle accelerator systems, *Physical Review Accelerators and Beams* **23**, 044601 (2020).